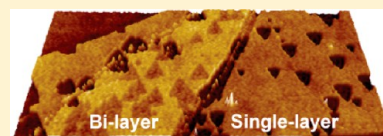


Anisotropic Etching of Atomically Thin MoS₂

Mahito Yamamoto,^{†,§} Theodore L. Einstein,[†] Michael S. Fuhrer,^{†,‡,*} and William G. Cullen[†][†]Materials Research Science and Engineering Center and Center for Nanophysics and Advanced Materials, Department of Physics, University of Maryland, College Park, Maryland 20742-4111, United States[‡]School of Physics, Monash University, Victoria 3800, Australia

Supporting Information

ABSTRACT: Exposure to oxygen at 300–340 °C results in triangular etch pits with uniform orientation on the surfaces of atomically thin molybdenum disulfide (MoS₂), indicating anisotropic etching terminating on lattice planes. The triangular pits grow laterally with oxidation time. The density of pits scarcely depends on oxidation time, temperature, and MoS₂ thickness but varies significantly from sample to sample, indicating that etching is initiated at native defect sites on the basal plane surface rather than activated by substrate effects such as charged impurities or surface roughness. Raman spectroscopy confirms that oxygen treatment produces no molybdenum oxide (MoO₃) below 340 °C. However, upon oxidation above 200 °C, the Raman A_{1g} mode upshifts and the linewidth decreases, indicating p-type doping of MoS₂. Oxidation at 400 °C results in complete conversion to MoO₃.



INTRODUCTION

Two-dimensional crystals of layered transition metal dichalcogenides have been of increasing interest for a wide variety of applications in electronics and optoelectronics.^{1,2} Field effect transistors (FET) based on thin molybdenum disulfide (MoS₂) flakes exhibit high on/off switching ratios of >10⁸^{3,4} and high carrier mobilities depending on thickness and dielectric environment.^{5,6} Carrier transport in atomically thin MoS₂ is sensitive to chemical adsorbates, making it a candidate for chemical sensor applications.^{7,8} Single-layer MoS₂ is a direct band gap semiconductor that emits strong photoluminescence⁹ and can be applied in photovoltaics, photodetectors, and photoemitters.^{10–12} Additionally, thanks to its huge surface-to-volume ratio, atomically thin MoS₂ could be a more efficient catalyst than bulk MoS₂ for the hydrogen-evolution reaction.¹³

Nanoscale control of edge structures offers a means to tune the electronic, optical, chemical, and catalytic properties of atomically thin two-dimensional materials. For example, the atomic-scale structure of graphene edges is predicted to have significant impact on the properties of graphene nanostructures, and progress toward atomically well-defined edges has been reported for graphene through chemical etching methods.^{14–17} Thermally activated metallic nanoparticles lead to crystallographic cutting of single- and few-layer graphene upon hydrogen treatment.^{14,15} Carbothermal reaction¹⁶ and hydrogen plasma treatment¹⁷ result in hexagonal etch pits on the surface of graphene. Similarly, control of edge structures is expected to lead to tunable properties of atomically thin MoS₂ nanostructures.^{18–26} The prismatic edges of semiconducting MoS₂ can exhibit metallic edge states^{18–21} and magnetism,^{20–22} with the properties sensitively dependent on the edge orientation and atomic reconstruction.^{20,21} The edge structure^{19,23} and number of active edge sites^{24–26} are also crucial for electrocatalytic activity of MoS₂.

However, whereas layer-by-layer thinning of MoS₂ has been reported,^{27–29} crystallographic etching of atomically thin MoS₂ has yet to be experimentally demonstrated. Here we show that oxygen treatment leads to triangular etch pits on the surfaces of atomically thin MoS₂. The pits have uniform orientations on the surfaces, indicating that MoS₂ is etched preferentially along the crystallographic directions of the zigzag edges with a preferential [that is, Mo-edge (10 $\bar{1}$ 0) or S-edge ($\bar{1}$ 010)] termination. The etch pits grow with increasing oxidation exposure, and the growth rate is larger for higher temperature. However, the density of etch pits is largely uncorrelated with oxidation time, oxidation temperature, and MoS₂ thickness but does vary significantly from sample to sample. These observations indicate that the oxidative etching in atomically thin MoS₂ on SiO₂ is initiated at intrinsic defect sites, similar to thick graphene (or graphite), rather than being activated by substrate effects such as charged impurities. Raman spectroscopy measurements indicate no formation of molybdenum oxide (MoO₃) after oxygen treatment of atomically thin MoS₂, at least below 340 °C. However, oxygen exposure above 200 °C results in upshift in the frequency and decrease in the linewidth of the Raman A_{1g} mode, which indicates that the electron density in single-layer MoS₂ is significantly diminished by oxygen treatment. Oxygen treatment at 400 °C does result in conversion of MoS₂ to MoO₃ platelets. Our results may signify an approach to create MoS₂ nanostructures with atomically well-defined edges by oxidation.

EXPERIMENTAL METHODS

Single- and few-layer MoS₂ were mechanically exfoliated onto 300 nm thick SiO₂ from MoS₂ bulk crystals using adhesive tape

Received: November 5, 2013

Published: November 12, 2013



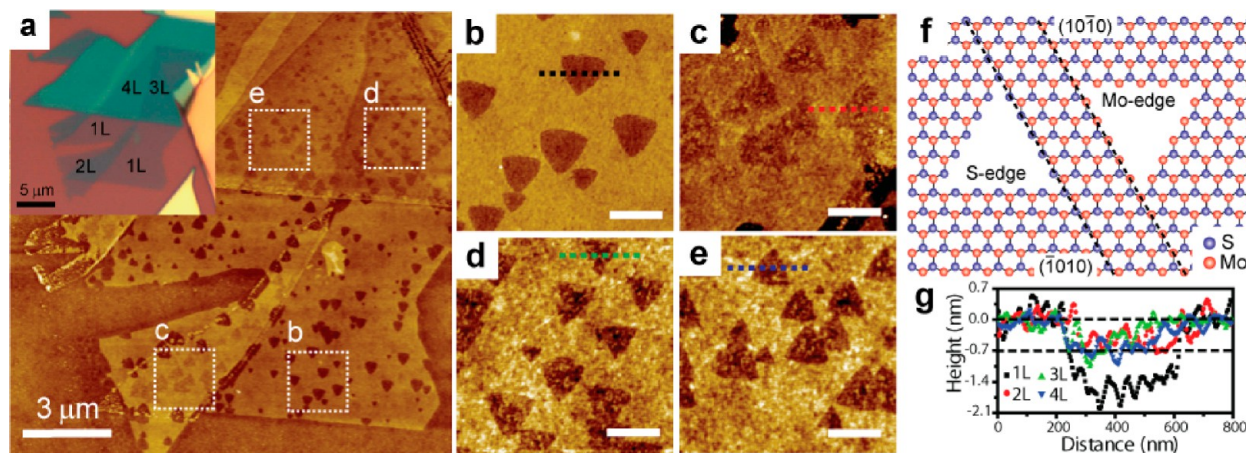


Figure 1. (a) An AFM image of single-layer (1L), bilayer (2L), trilayer (3L), and four-layer (4L) MoS₂ on SiO₂ after oxidation at 320 °C for 3 h. The inset shows an optical image of this flake before oxidation. (b–e) Close-up images of the areas surrounded by dashed lines on (b) 1L, (c) 2L, (d) 3L, and (e) 4L in the panel (a). The scale bars are 500 nm. (f) Schematic drawing of hexagonal lattice of the MoS₂ structure with triangular pits. Two dashed lines indicate the $(\bar{1}0\bar{1}0)$ S and $(10\bar{1}0)$ Mo edges. The little blue circles correspond to 2 S atoms in outer constituent layers above and below the Mo (red circles) interior constituent layer. Evidence for MoS₂ nanocrystal islands suggests that the Mo $(10\bar{1}0)$ edge is more stable, and that it is decorated by S atoms in one of two possible configurations that cannot be distinguished in our experiment as described in text. (g) Profiles of pits along the dashed lines in (b–e).

(3M Water-Soluble Wave Solder Tape 5414). The thicknesses of MoS₂ were identified by optical contrast, atomic force microscopy (AFM), and Raman spectroscopy.^{30,31} To remove adhesive residue, all samples were annealed in an H₂/Ar mixture for 2 h at 350 °C. The flow rates of Ar and H₂ are 1.7 and 1.8 L/min, respectively. This hydrogen treatment leads to no chemical modification of the MoS₂ basal plane (see Supporting Information for an AFM image and Raman spectra of MoS₂). After preannealing MoS₂ samples in H₂, they were exposed to an Ar/O₂ mixture at temperatures ranging from 27 to 400 °C. The flow rates of Ar and O₂ are 1.0 and 0.7 L/min, respectively. The nanoscale structure of oxidized MoS₂ was characterized by AFM in tapping mode using silicon cantilevers with a nominal tip radius of >10 nm (NCH, Nanoworld), and the composition and oxidation state were determined using Raman spectroscopy (Horiba Jobin Yvon Raman microscope) with 2400 gratings per mm and a solid state laser with a fixed excitation wavelength of 532 nm.

RESULTS AND DISCUSSION

Figure 1a shows a typical AFM topographic image of atomically thin MoS₂ supported on SiO₂ after oxygen annealing at 320 °C for 3 h (see the inset for an optical image of this flake). The oxygen treatment results in etch pits on the surfaces of single- and few-layer MoS₂. We observe the formation of etch pits even after air annealing (see Supporting Information for an AFM image), suggesting that the etching process is independent of the partial pressure of oxygen gas. As shown in Figure 1b–e, the shape of the pits is triangular and their orientations are identical over each atomically flat terrace. These observations indicate that the triangular shapes of the pits reflect the lattice of the MoS₂ basal plane surface and that the edges of the pits are along the zigzag directions with only a single chemical termination, that is, terminated on either the Mo-edge ($10\bar{1}0$) or S-edge ($\bar{1}0\bar{1}0$) (see Figure 1f). The observation of only three preferred edge orientations rules out armchair-oriented edges for which there are six possible identical edges. Our experiments are unable to resolve whether the preferred edge is the Mo-edge or S-edge; however, evidence from other studies

points to Mo-edge ($10\bar{1}0$),^{18,19,23,26} though the exact structure of the reconstructed edge (and locations of additional sulfur atoms terminating the Mo-edge) likely depends on the chemical environment and substrate.^{19,23,26} Further work using high-resolution transmission electron microscopy or scanning tunneling microscopy could resolve the issue and also elucidate the electronic and magnetic properties of these edges.

Figure 1g shows the profiles of the pits along the dashed lines in Figure 1b–e. The pits are mostly single-layer-deep (~ 0.7 nm) on single- and few-layer MoS₂, indicating a very high degree of anisotropy in etching along the basal plane versus the *c*-axis, though we do occasionally observe double-layer-deep pits on few-layer MoS₂ samples (see Figure 3e,f). (The larger depth of the pits on single-layer MoS₂ in Figure 1g is an artifact caused by the limitation of the tapping mode AFM to determine the thickness of an atomically thin membrane on rough SiO₂.³²) The AFM images do not show any clear sign of the reaction products (presumably MoO₃); we discuss this in more detail below.

Our MoS₂ crystals are expected to have a 2H structure,^{1,2} where the triangular lattices of adjacent layers are 180°-inverted relative to each other. Therefore, the triangular pits formed on the surfaces are also expected to have 180°-inverted orientations among even and odd numbers of layers. Such trends can be seen in Figure 1a. However, we also observe the triangular pits with same orientations on even and odd layer-number-thickness regions (see Supporting Information for an AFM image), suggesting that it is the top surface that is continuous across the layer-number-thickness boundary. Because of this ambiguity, we cannot be certain of the correlation between the stacking order of MoS₂ layers and the orientations of the triangular pits; however, the observations of only a single etch-pit orientation within a single terrace, and the observation of opposite orientations for different layer thicknesses within a single crystal, suggests strongly that the termination is globally determined to be along only one of the Mo or S terminated zigzag edges.

In Figure 2a–d, we show AFM images of a MoS₂ flake of single- and bilayer thickness after oxidation at 320 °C for 1, 3,

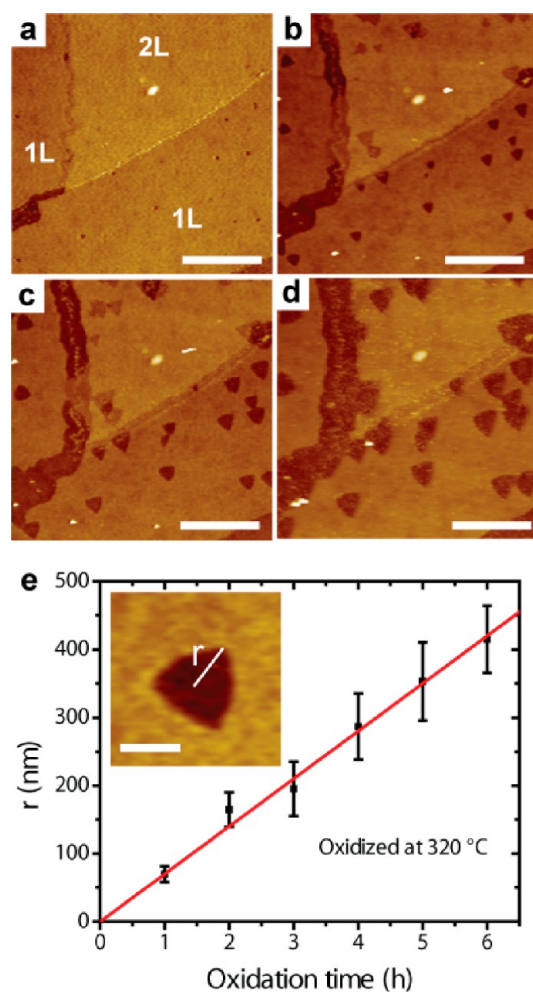


Figure 2. (a–d) AFM images of 1L and 2L MoS₂ oxidized at 320 °C for (a) 1, (b) 3, (c) 4, and (d) 6 h. The scale bars are 2 μm . (e) The average distance r from the center to the apex of triangular pits as a function of oxidation time. The red line is fit. The inset is an AFM image of a typical triangular pit formed on single-layer MoS₂ after oxidation for 4 h. The scale bar is 300 nm.

4, and 6 h. After oxidation for an hour, etch pits with an average size of $6.3 \times 10^3 \text{ nm}^2$ are formed on the surfaces (Figure 2a). Additional oxygen treatment leads to lateral growth of the triangular pits, as shown in Figure 2b–d. The distance r from the center to the apex of the triangular pits increases almost linearly with a growth rate of approximately 70 nm/h, as shown in Figure 2e, but the density of pits is nearly constant during the oxygen treatment, indicating that the oxidative etching is not initiated homogeneously but at specific sites on the surface of atomically thin MoS₂.

Figure 3a–d shows AFM images of MoS₂ samples of various thicknesses after oxidation at 320 °C for 1 h. In Figure 3a, the density of etch pits formed on the single-layer MoS₂ film is $7.5 \times 10^6 \text{ cm}^{-2}$, while the pit density on single-layer MoS₂ in Figure 3b is 2 orders of magnitude larger than that in Figure 3a. Figure 3c shows a MoS₂ flake of single- to 4-layer thickness with etch pits on the surfaces. The density of pits on 4-layer MoS₂ is $3.5 \times 10^8 \text{ cm}^{-2}$, which is larger than the densities on surfaces of single-layer ($9.0 \times 10^7 \text{ cm}^{-2}$) and trilayer ($2.7 \times 10^8 \text{ cm}^{-2}$)

parts. Figure 3d shows an example of a large pit density of $\sim 10^9 \text{ cm}^{-2}$ observed on 8- and 9-layer MoS₂. These observations suggest that the density of pits formed upon oxidation has no obvious correlation with MoS₂ thickness but shows significant sample-to-sample variations. Figure 3e–g shows AFM images of single- and bilayer MoS₂ after oxidation at 300 °C for 4 h, 320 °C for 3 h, and 340 °C for 2 h, respectively. Higher-temperature oxygen annealing leads to larger etch pits on the surfaces. However, the density of pits on single-layer MoS₂ oxidized at 340 °C is 1 order of magnitude smaller than when oxidized at 300 and 320 °C. Hence, the density of pits exhibits no obvious simple correlation with the oxidation temperature.

The observed oxidative behaviors of atomically thin MoS₂ on SiO₂ are in sharp contrast with oxidation of graphene supported on the same SiO₂ surface. Oxygen treatment of graphene on SiO₂ results in circular etch pits on the surface.^{33,34} However, unlike atomically thin MoS₂, the oxidative etching of SiO₂-supported graphene is strongly thickness-dependent with single-layer being the most reactive. Furthermore, the etch pits in single-layer graphene on SiO₂ form homogeneously on the surface, and the number of pits increases with oxidation time and temperature. The anomalous reactivity of single-layer graphene on SiO₂ is due to charge inhomogeneity induced by charged impurities in SiO₂.^{34,35} The effect of the charged impurities is significantly reduced with increasing graphene thickness. Thus, for thicker graphene (or graphite), the etching is predominantly activated by native defects in the crystal, and the etch pits have nearly uniform lateral sizes and mostly one-layer depth.³⁶ The oxidation of atomically thin MoS₂ appears similar in character to the oxidation of graphite crystal surfaces, rather than graphene on SiO₂. We thus suppose that the oxidative etching of atomically thin MoS₂ is similarly initiated at defect sites on the surfaces. In Figure 3h, we show a histogram of the density of pits formed on single- and few-layer MoS₂ after oxidation at various temperatures. The pit density ranges from 10^6 to 10^9 cm^{-2} , which corresponds with the previously reported density of intrinsic vacancy defects and substitutional atoms such as tungsten and vanadium in the natural MoS₂ crystal,^{37,38} indicating that such defects could be responsible for initiating etching.

Previous scanning probe microscopy³⁹ and X-ray photoemission measurements⁴⁰ have shown that high-temperature oxidation leads to the formation of thin MoO₃ films on the basal plane surface of bulk MoS₂. The Raman investigations of microcrystalline MoS₂ have revealed that oxygen exposure results in a peak at 820 cm^{-1} that is a stretching mode of the terminal oxygen atoms (O–M–O) in MoO₃, and the normalized intensity of the mode increases with increasing oxidation temperature above 100 °C.⁴¹ We observe a peak at 820 cm^{-1} in pristine single-layer MoS₂, as shown in Figure 4a (black line). However, the peak intensity at 820 cm^{-1} relative to the Si peak at $\sim 520 \text{ cm}^{-1}$ rarely changes after oxygen treatment, even at 340 °C for 2 h as shown in Figure 4a (red line). We conclude that the peak at 820 cm^{-1} in oxidized MoS₂ is not the stretching mode in MoO₃ but rather the second-order A_{1g} mode of MoS₂.⁴² This is also supported by the absence of other MoO₃-related peaks such as 285 and 995 cm^{-1} in the Raman spectrum of oxidized MoS₂. Furthermore, we find the thickness of MoS₂ does not change after oxidation below 340 °C, suggesting that no MoO₃ films are formed. Thus, Raman spectroscopy clearly demonstrates that single-layer MoS₂ remains after oxidation up to 340 °C but shows no evidence of MoO₃ formation, though we cannot rule out the possibility

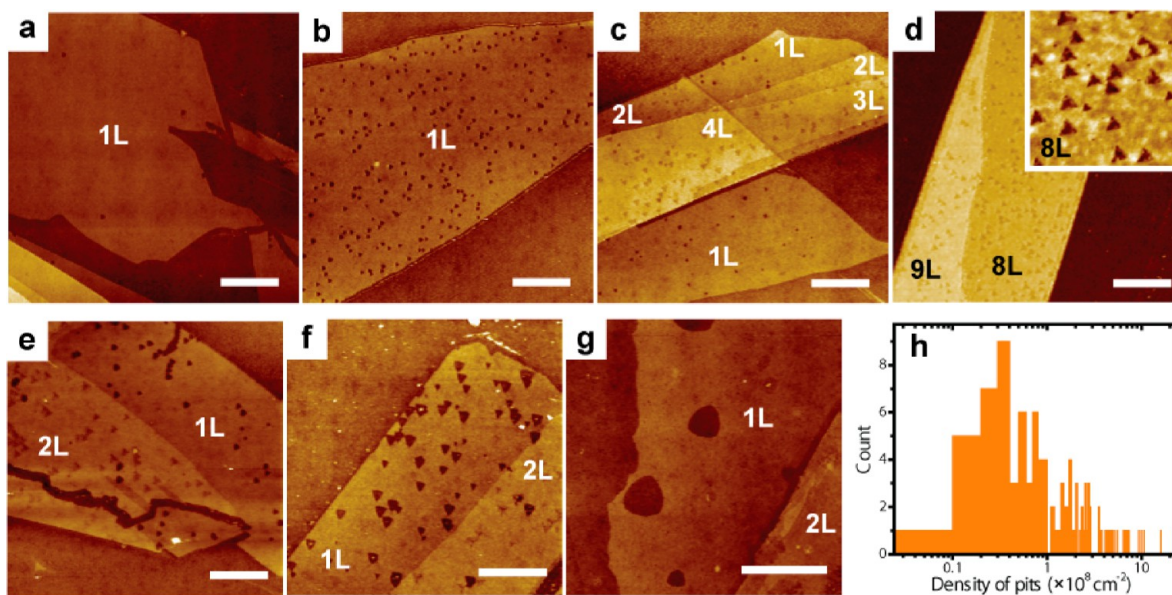


Figure 3. (a–d) AFM images of MoS₂ samples of 1L, 2L, 3L, 4L, 8-layer (8L), and 9-layer (9L) thicknesses after oxidation at 320 °C for 2 h. The scale bars are 2 μm. The inset in (d) is a 1 μm × 1 μm area in the 8L region, showing triangular pits. (e–g) AFM images of 1L and 2L MoS₂ on SiO₂ after oxidation at (e) 300 °C for 4 h, (f) 320 °C for 3 h, and (g) 340 °C for 2 h. The scale bars are 2 μm. (h) Histogram of the density of pits formed on single- and few-layer MoS₂ oxidized at various temperatures.

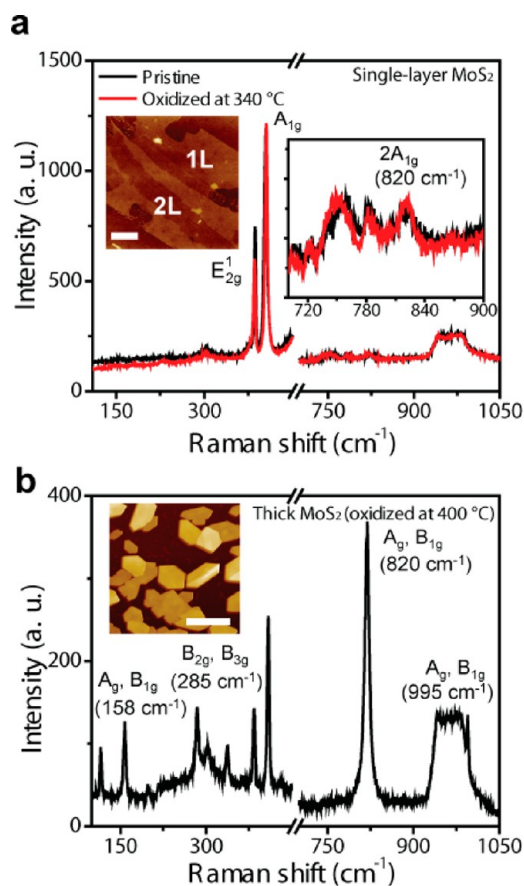


Figure 4. (a) Raman spectra of single-layer MoS₂ before (black line) and after (red line) oxidation at 340 °C for 2 h. The inset on the right expands the Raman spectra near 820 cm⁻¹. The inset on the left is a corresponding AFM image of 1L and 2L MoS₂. The scale bar is 1 μm. (b) A Raman spectrum of thick MoS₂ oxidized at 400 °C for 10 min, showing MoO₃-related peaks. The inset is an AFM image of oxidized thick MoS₂ crystals at 400 °C. The scale bar is 1 μm.

that the Raman MoO₃ peaks are simply too weak to be detected.

We find that oxidation above 350 °C rapidly etches away single- and few-layer MoS₂. However, we find that high-temperature oxidation of thicker MoS₂ (>40 nm in thickness) above 400 °C leads to significant structural and chemical modification. The inset of Figure 4b is an AFM image of 40 nm thick MoS₂ oxidized at 400 °C for 10 min. The thick MoS₂ decomposes into smaller crystals with a lateral size of about 300 nm in length (see also Supporting Information for optical images of a thick MoS₂ flake before and after oxidation). The Raman spectrum of the crystal (Figure 4b) shows MoO₃-related modes of 189, 285, 820, and 995 cm⁻¹ (see Supporting Information for Raman spectra of oxidized MoS₂ near 995 cm⁻¹),⁴¹ corroborating that MoO₃ is formed by high-temperature oxidation of thick MoS₂.

Oxygen treatment is expected to modify significantly the electronic properties of atomically thin MoS₂. Indeed, exposing few-layer MoS₂ FET devices to oxygen gas leads to considerable decrease in electron density and conductivity.^{43,44} We investigate the effects of oxygen on the carrier concentrations in MoS₂ using Raman spectroscopy. Previous Raman measurement of single-layer MoS₂ using electrolyte gating, combined with the density functional theory calculations, has revealed that the Raman A_{1g} mode downshifts and its linewidth increases with increasing electron density due to electron–phonon interactions.⁴⁵ In contrast, the E¹_{2g} phonon is less sensitive to electron concentration than the A_{1g} phonon. In Figure 5a, we show the Raman E¹_{2g} and A_{1g} modes of single-layer MoS₂ before and after oxidation at temperatures of 200, 300, and 340 °C for 2 h. Oxygen treatment above 200 °C results in the upshift of the frequency and the decrease of the linewidth of the A_{1g} mode, indicating that electrons transfer presumably from MoS₂ to adsorbed oxygen molecules. Figure 5b,c shows the frequencies and linewidths of the Raman E¹_{2g} and A_{1g} modes as functions of the oxidation temperature. The positions of the E¹_{2g} and the A_{1g} peaks do not shift measurably

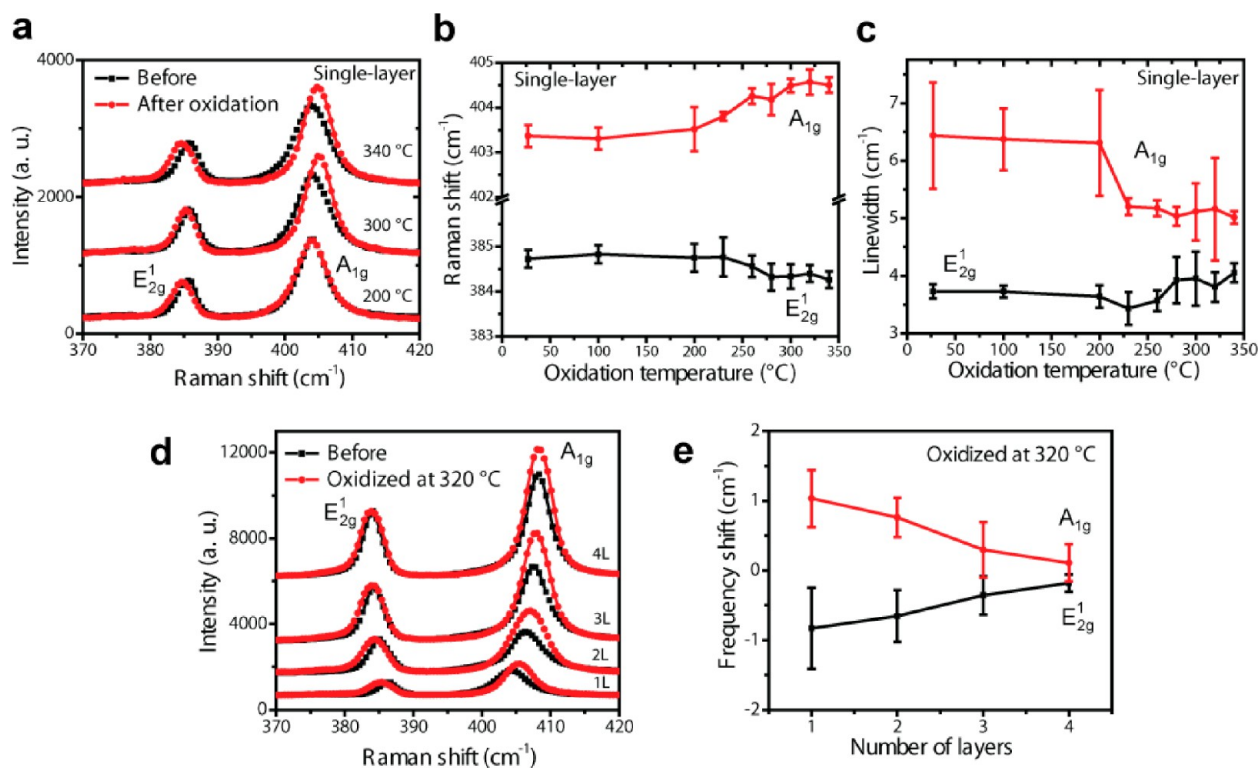


Figure 5. (a) The Raman E_{2g}^1 and A_{1g} modes of single-layer MoS_2 before (black) and after (red) oxidation at 200, 300, and 340 °C for 2 h. (b,c) Frequencies (b) and linewidths (c) of the E_{2g}^1 and A_{1g} modes versus oxidation temperature. (d) Raman E_{2g}^1 and A_{1g} modes of 1L, 2L, 3L, and 4L MoS_2 after oxidation at 320 °C for 2 h. (e) Shifts in the peak position of the E_{2g}^1 and A_{1g} modes as functions of thickness.

after oxygen annealing below 200 °C. However, above 200 °C the E_{2g}^1 mode slightly decreases while the A_{1g} mode increases with temperature up to 404.5 cm^{-1} at 340 °C. Furthermore, as shown in Figure 5c, the line width of the A_{1g} mode abruptly decreases above 200 °C, while the E_{2g}^1 mode shows nearly constant line width over temperature. Although the cause of the shift in the E_{2g}^1 mode is unclear, these results suggest that below 200 °C the electron transfer upon oxidation is minor but with increasing temperature there is sizable electron withdrawal by oxygen treatment. Using the results by Chakraborty et al.,⁴⁵ we estimate the density of electrons withdrawn to be of order 10^{13} cm^{-2} for 340 °C oxidation.

In Figure 5d, we show the Raman E_{2g}^1 and A_{1g} modes of single-, bi-, tri-, and four-layer MoS_2 after oxidation at 320 °C for 2 h. The oxidation results in upshift of the A_{1g} mode and downshift of the E_{2g}^1 mode of single- and few-layer MoS_2 . However, as shown in Figure 5d, the shifts of the E_{2g}^1 and A_{1g} modes decrease with increasing thickness. This indicates that electron transfer from atomically thin MoS_2 by oxygen treatment is a surface effect, which is consistent with observations that atomically thin MoO_3 is not formed upon oxidation below 340 °C.

CONCLUSIONS

In summary, we find that oxygen treatment of atomically thin MoS_2 results in triangular etch pits whose edges are along zigzag directions which other evidence suggests have Mo orientations. The pit density is uncorrelated with oxidation temperature, time, and MoS_2 thickness, indicating that the oxidative etching is initiated via intrinsic defects in MoS_2 rather than substrate effects such as charged impurities or surface roughness. We further find that oxygen exposure leads to

sizable electron transfer from MoS_2 surfaces above 200 °C but produces no MoO_3 below 340 °C. Our results can be applied to create MoS_2 nanostructures with atomically well-defined edges and provide insight into the oxidative reactivity of atomically thin MoS_2 on substrates.⁴⁶

ASSOCIATED CONTENT

Supporting Information

An AFM image and a Raman spectrum of MoS_2 after H_2 treatment, an AFM image of MoS_2 after air annealing, an additional AFM image of oxidized MoS_2 with etch pits, optical images, and an AFM image of thick MoS_2 before and after oxidation, and Raman spectra of thick MoS_2 before and after oxidation. This material is available free of charge via the Internet at <http://pubs.acs.org>.

AUTHOR INFORMATION

Corresponding Author

*E-mail: michael.fuhrer@monash.edu. Phone: +61 (3) 9905 1353. Fax: +61 (3) 9905 3637.

Present Address

[§]WPI Center for Materials Nanoarchitectonics (WPI-MANA), National Institute for Materials Science, Tsukuba, Ibaraki 305-0044, Japan.

Notes

The authors declare no competing financial interest.

ACKNOWLEDGMENTS

This work has been supported by the University of Maryland NSF-MRSEC and MRSEC shared facilities under Grant DMR 05-20741, NSF Grants CHE 07-50334 and 13-05892 (TLE), and the U.S. Office of Naval Research MURI program. M.S.F. is

the recipient of an Australian Research Council Laureate Fellowship (Project Number FL120100038).

REFERENCES

- (1) Wang, Q. H.; Kalantar-Zadeh, K.; Kis, A.; Coleman, J. N.; Strano, M. S. Electronics and Optoelectronics of Two-Dimensional Transition Metal Dichalcogenides. *Nat. Nanotechnol.* **2012**, *7*, 699–712.
- (2) Chhowalla, M.; Shin, H. S.; Eda, G.; Li, L. -J.; Loh, K. P.; Zhang, H. The Chemistry of Two-Dimensional Layered Transition Metal Dichalcogenide Nanosheets. *Nature Chem.* **2013**, *5*, 263–275.
- (3) Radisavljevic, B.; Radenovic, A.; Brivio, J.; Giacometti, V.; Kis, A. Single-Layer MoS₂ Transistors. *Nat. Nanotechnol.* **2011**, *6*, 147–150.
- (4) Ayari, A.; Cobas, E.; Ogundadegbe, O.; Fuhrer, M. S. Realization and Electrical Characterization of Ultrathin Crystals of Layered Transition-Metal Dichalcogenides. *J. Appl. Phys.* **2007**, *101*, 014507.
- (5) Kim, S.; Konar, A.; Hwang, W.-S.; Lee, J. H.; Lee, J.; Yang, J.; Jung, C.; Kim, H.; Yoo, J. -B.; Choi, J. -Y.; et al. High-Mobility and Low-Power Thin-Film Transistors Based on Multilayer MoS₂ Crystals. *Nat. Commun.* **2012**, *3*, 1011.
- (6) Bao, W.; Cai, X.; Kim, D.; Sridhara, K.; Fuhrer, M. S. High Mobility Ambipolar MoS₂ Field-Effect Transistors: Substrate and Dielectric Effects. *Appl. Phys. Lett.* **2013**, *102*, 042104.
- (7) Li, H.; Yin, Z.; He, Q.; Li, H.; Huang, X.; Lu, G.; Fam, D. W. H.; Tok, A. L. Y.; Zhang, Q.; Zhang, H. Fabrication of Single- and Multilayer MoS₂ Film-Based Field-Effect Transistors for Sensing NO at Room Temperature. *Small* **2012**, *8*, 63–67.
- (8) Perkins, F. K.; Friedman, A. L.; Cobas, E.; Campbell, P. M.; Jernigan, G. G.; Jonker, B. T. Chemical Vapor Sensing with Monolayer MoS₂. *Nano Lett.* **2013**, *13*, 668–673.
- (9) Mak, K. F.; Lee, C.; Hone, J.; Shan, J.; Heinz, T. F. Atomically Thin MoS₂: A New Direct-Gap Semiconductor. *Phys. Rev. Lett.* **2010**, *105*, 136805.
- (10) Fontana, M.; Deppe, T.; Boyd, A. K.; Rinzan, M.; Liu, A. Y.; Paranjape, M.; Barbara, P. Electron-Hole Transport and Photovoltaic Effect in Gated MoS₂ Schottky Junctions. *Sci. Rep.* **2013**, *3*, 1634.
- (11) Yin, Z.; Li, H.; Li, H.; Jiang, L.; Shi, Y.; Sun, Y.; Lu, G.; Zhang, Q.; Chen, X.; Zhang, H. Single-Layer MoS₂ Phototransistors. *ACS Nano* **2012**, *6*, 74–80.
- (12) Sundaram, R. S.; Engel, M.; Lombardo, A.; Krupke, R.; Ferrari, A. C.; Avouris, P.; Steiner, M. Electroluminescence in Single Layer MoS₂. *Nano Lett.* **2013**, *13*, 1416–1421.
- (13) Voiry, D.; Yamaguchi, H.; Li, J.; Silva, R.; Alves, D. C. B.; Fujita, T.; Chen, M.; Asefa, T.; Shenoy, V.; Eda, G. Enhanced Catalytic Activity in Strained Chemically Exfoliated WS₂ Nanosheets for Hydrogen Evolution. *Nat. Mater.* **2013**, *12*, 850–855.
- (14) Datta, S. S.; Strachan, D. R.; Khamis, S. M.; Johnson, A. T. C. Crystallographic Etching of Few-Layer Graphene. *Nano Lett.* **2008**, *8*, 1912–1915.
- (15) Campos, L. C.; Manfrinato, V. R.; Sanchez-Yamagishi, J. D.; Kong, J.; Jarillo-Herrero, P. Anisotropic Etching and Nanoribbon Formation in Single-Layer Graphene. *Nano Lett.* **2009**, *9*, 2600–2604.
- (16) Nemes-Incze, P.; Magda, G.; Kamarás, K.; Biró, L. P. Crystallographically Selective Nanopatterning of Graphene on SiO₂. *Nano Res.* **2010**, *3*, 110–116.
- (17) Yang, R.; Zhang, L.; Wang, Y.; Shi, Z.; Shi, D.; Gao, H.; Wang, E.; Zhang, G. An Anisotropic Etching Effect in the Graphene Basal Plane. *Adv. Mater.* **2010**, *22*, 4014–4019.
- (18) Helveg, S.; Lauritsen, J. V.; Lægsgaard, E.; Stensgaard, I.; Nørskov, J. K.; Clausen, B. S.; Topsøe, H.; Besenbacher, F. Atomic-Scale Structure of Single-Layer MoS₂ Nanoclusters. *Phys. Rev. Lett.* **2000**, *84*, 951–954.
- (19) Bollinger, M. V.; Jacobsen, K. W.; Nørskov, J. K. Atomic and Electronic Structure of MoS₂ Nanoparticles. *Phys. Rev. B* **2003**, *67*, 085410.
- (20) Li, Y.; Zhou, Z.; Zhang, S.; Chen, Z. MoS₂ Nanoribbons: High Stability and Unusual Electronic and Magnetic Properties. *J. Am. Chem. Soc.* **2008**, *130*, 16739–16744.
- (21) Botello-Méndez, A. R.; López-Urías, F.; Terrones, M.; Terrones, H. Metallic and Ferromagnetic Edges in Molybdenum Disulfide Nanoribbons. *Nanotechnology* **2009**, *20*, 325703.
- (22) Zhang, J.; Soon, J. M.; Loh, K. P.; Yin, J.; Ding, J.; Sullivan, M. B.; Wu, P. Magnetic Molybdenum Disulfide Nanosheet Films. *Nano Lett.* **2007**, *7*, 2370–2376.
- (23) Vojvodic, A.; Hinnemann, B.; Nørskov, J. K. Magnetic Edge States in MoS₂ Characterized Using Density-Functional Theory. *Phys. Rev. B* **2009**, *80*, 125416.
- (24) Jaramillo, T. F.; Jørgensen, K. P.; Bonde, J.; Nielsen, J. H.; Horch, S.; Chorkendorff, I. Identification of Active Edge Sites for Electrochemical H₂ Evolution from MoS₂ Nanocatalysts. *Science* **2007**, *317*, 100–102.
- (25) Kibsgaard, J.; Chen, Z.; Reinecke, B. N.; Jaramillo, T. F. Engineering the Surface Structure of MoS₂ to Preferentially Expose Active Edge Sites for Electrocatalysis. *Nat. Mater.* **2012**, *11*, 963–969.
- (26) Moses, P. G.; Hinnemann, B.; Topsøe, H.; Nørskov, J. K. The Hydrogenation and Direct Desulfurization Reaction Pathway in Thiophene Hydrodesulfurization over MoS₂ Catalysts at Realistic Conditions: A Density Functional Study. *J. Catal.* **2007**, *248*, 188–203.
- (27) Castellanos-Gomez, A.; Barkelid, M.; Goossens, A. M.; Calado, V. E.; van der Zant, H. S. J.; Steele, G. A. Laser-Thinning of MoS₂: On Demand Generation of a Single-Layer Semiconductor. *Nano Lett.* **2012**, *12*, 3187–3192.
- (28) Huang, Y.; Wu, J.; Xu, X.; Ho, Y.; Ni, G.; Zou, Q.; Koon, G. K. W.; Zhao, W.; Castro Neto, A. H.; Eda, G.; et al. An Innovative Way of Etching MoS₂: Characterization and Mechanistic Investigation. *Nano Res.* **2013**, *6*, 200–207.
- (29) Liu, Y.; Nan, H.; Wu, X.; Pan, W.; Wang, W.; Bai, J.; Zhao, W.; Sun, L.; Wang, X.; Ni, Z. Layer-by-Layer Thinning of MoS₂ by Plasma. *ACS Nano* **2013**, *7*, 4202–4209.
- (30) Lee, C.; Yan, H.; Brus, L. E.; Heinz, T. F.; Hone, J.; Ryu, S. Anomalous Lattice Vibrations of Single- and Few-Layer MoS₂. *ACS Nano* **2010**, *4*, 2695–2700.
- (31) Li, S.-L.; Miyazaki, H.; Song, H.; Kuramochi, H.; Nakaharai, S.; Tsukagoshi, K. Quantitative Raman Spectrum and Reliable Thickness Identification for Atomic Layers on Insulating Substrates. *ACS Nano* **2012**, *6*, 7381–7388.
- (32) Nemes-Incze, P.; Osváth, Z.; Kamarás, K.; Biró, L. P. Anomalies in Thickness Measurements of Graphene and Few Layer Graphite Crystals by Tapping Mode Atomic Force Microscopy. *Carbon* **2008**, *46*, 1435–1422.
- (33) Liu, L.; Ryu, S.; Tomasik, M. R.; Stolyarova, E.; Jung, N.; Hybertsen, M. S.; Steigerwald, M. L.; Brus, L. E.; Flynn, G. W. Graphene Oxidation: Thickness-Dependent Etching and Strong Chemical Doping. *Nano Lett.* **2008**, *8*, 1965–1970.
- (34) Yamamoto, M.; Einstein, T. L.; Fuhrer, M. S.; Cullen, W. G. Charge Inhomogeneity Determines Oxidative Reactivity of Graphene on Substrates. *ACS Nano* **2012**, *6*, 8335–8341.
- (35) Wang, Q. H.; Jin, Z.; Kim, K. K.; Hilmer, A. J.; Paulus, G. L. C.; Shih, C.-J.; Ham, M.-H.; Sanchez-Yamagishi, J. D.; Watanabe, K.; Taniguchi, T.; et al. Understanding and Controlling the Substrate Effect on Graphene Electron-Transfer Chemistry via Reactivity Imprint Lithography. *Nature Chem.* **2012**, *4*, 724–732.
- (36) Lee, S. M.; Lee, Y. H.; Hwang, Y. G.; Hahn, J. R.; Kang, H. Defect-Induced Oxidation of Graphite. *Phys. Rev. Lett.* **1999**, *82*, 217–220.
- (37) Ha, J. S.; Roh, H.-S.; Park, S.-J.; Yi, J.-Y.; Lee, E.-H. Scanning Tunneling Microscopy Investigation of the Surface Structures of Natural MoS₂. *Surf. Sci.* **1994**, *315*, 62–68.
- (38) Whangbo, M.-H.; Ren, J.; Magonov, S. N.; Bengel, H.; Parkinson, B. A.; Suna, A. On the Correlation between the Scanning Tunneling Microscopy Image Imperfections and Point Defects of Layered Chalcogenides 2H-MX₂ (M = Mo, W; X = S, Se). *Surf. Sci.* **1995**, *326*, 311–326.
- (39) Wang, J.; Rose, K. C.; Lieber, C. M. Load-Independent Friction: MoO₃ Nanocrystal Lubricants. *J. Phys. Chem. B* **1999**, *103*, 8405–8409.

- (40) Lince, J. R.; Frantz, P. P. Anisotropic Oxidation of MoS₂ Crystallites Studied by Angle-Resolved X-Ray Photoelectron Spectroscopy. *Tribol. Lett.* **2000**, *9*, 211–218.
- (41) Windom, B. C.; Sawyer, W. G.; Hahn, D. W. A Raman Spectroscopic Study of MoS₂ and MoO₃: Applications to Tribological Systems. *Tribol. Lett.* **2011**, *42*, 301–310.
- (42) Chen, J. M.; Wang, C. S. Second Order Raman Spectrum of MoS₂. *Solid State Commun.* **1974**, *14*, 857–860.
- (43) Qiu, H.; Pan, L.; Yao, Z.; Li, J.; Shi, Y.; Wang, X. Electrical Characterization of Back-Gated Bi-Layer MoS₂ Field-Effect Transistors and the Effect of Ambient on Their Performances. *Appl. Phys. Lett.* **2012**, *100*, 123104.
- (44) Park, W.; Park, J.; Jang, J.; Lee, H.; Jeong, H.; Cho, K.; Hong, S.; Lee, T. Oxygen Environmental and Passivation Effects on Molybdenum Disulfide Field Effect Transistors. *Nanotechnology* **2013**, *24*, 095202.
- (45) Chakraborty, B.; Bera, A.; Muthu, D. V. S.; Bhowmick, S.; Waghmare, U. V.; Sood, A. K. Symmetry-Dependent Phonon Renormalization in Monolayer MoS₂ Transistor. *Phys. Rev. B* **2012**, *85*, 161403(R).
- (46) Note added. We became aware of similar works after submission of this paper.^{47,48}
- (47) Zhou, H.; Yu, F.; Liu, Y.; Zou, X.; Cong, C.; Qiu, C.; Yu, T.; Yan, Z.; Shen, X.; Sun, L.; et al. Thickness-Dependent Patterning of MoS₂ Sheets with Well-Oriented Triangular Pits by Heating in Air. *Nano Res.* **2013**, *6*, 703–711.
- (48) Wu, J.; Li, H.; Yin, Z.; Li, H.; Liu, J.; Cao, X.; Zhang, Q.; Zhang, H. Layer Thinning and Etching of Mechanically Exfoliated MoS₂ Nanosheets by Thermal Annealing in Air. *Small* **2013**, *9*, 3314–3319.